Energy Stress of Surge Arresters Due to Temporary Overvoltages

B. Filipović-Grčić, I. Uglešić, V. Milardić, A. Xemard, A. Guerrier

Abstract-- **The paper presents a method for selecting the rated voltage of a metal oxide surge arresters (MOSA) based on the calculation of energy stresses. The electrical behaviour of gapless MOSA under temporary overvoltages (TOV) is important when selecting the rated voltage of MOSA. The study of the appropriate MOSA model is conducted for the evaluation of energy stresses due to TOV. The resistive part of the leakage current was derived from the voltage-current (*U-I*) characteristic for AC voltage that was gained during the laboratory tests. The MOSA model was implemented in the study of energy stresses of station arresters that are installed at both terminals of a compact upgraded line. By implementing the proposed method MOSA with relatively low protection level can be selected without being overstressed by TOV and thus the overvoltage protection of compact line can be improved.**

Keywords: **TOV, MOSA, energy stress, laboratory measurements, compact line, EMTP-RV, rated voltage selection.**

I. Introduction

So far the voltage rating of station MOSAs has been usually chosen higher than the amplitude of the TOV which can occur in the system. This approach leads to the use of MOSAs with high protection levels, especially if the system is not solidly grounded, which do not reduce the level of slow-front overvoltages (SFO) and fast-front overvoltages as efficiently as MOSAs with lower protection level would do. SFO due to energization or reclosing of the line may be reduced by using various techniques like point-on-the-wave switching or circuit breakers (CBs) equipped with pre-insertion resistors, but SFO due to faults on compact or upgraded lines might get critical. Obviously they cannot be reduced by the techniques listed above and the use of station MOSAs with a low protection level at the terminals of the line might be the only option [1], [2]. This low protection level requires the use of MOSAs whose rated voltage might be below the level of TOV and, consequently, the MOSA energy stress has to be determined accurately. Therefore, in the first part of the paper laboratory measurements were performed in order to obtain MOSA model for calculation of energy stress due to TOV.

B. Filipović-Grčić, I. Uglešić and V. Milardić are with are with Faculty of Electrical Engineering and Computing, University of Zagreb, Croatia (e-mail of corresponding author: bozidar.filipovic-grcic@fer.hr).
A. Xemard is with EDF R&D, Paris, France (alain.xemard@edf.fr).
A. Guerrier is with RTE, Paris, France (arnaud.guerrier@rte-france.com).

Paper submitted to the International Conference on Power Systems Transients (IPST2011) in Delft, the Netherlands June 14-17, 2011

II. Laboratory Measurements

In order to determine the behaviour of MOSA under TOV laboratory measurements were conducted on MOSA whose continuous operating and rated voltages are U_c=36 kV and U_r=45 kV, respectively. A laboratory circuit used for the measurement of the *U-I* characteristic under AC voltage is shown in Fig. 1.

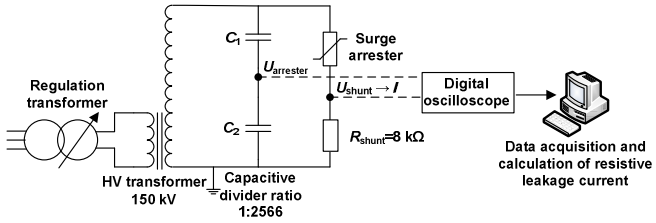

Fig. 1. Experimental circuit for the measurement of leakage current

A capacitive divider was used for measurement of voltage applied on MOSA, and the total leakage current signal was obtained from a shunt resistance R_{shunt}. The voltage signals were recorded using a digital oscilloscope and the data was saved in a computer. The total leakage current consists of a resistive and a capacitive part. A method for calculation of the resistive part of leakage current was developed in MATLAB software. A method is based on compensation technique [3]. The applied voltage contains harmonic components:

$$u = \sum_n U_n \sin(n\omega t + \Phi_n) \quad (1)$$

where

n – the rank of the harmonics (n=1 corresponds to the fundamental component);
U_n – voltage peak value of the n-th harmonic component;
Φ_n – phase angle of the n-th harmonic component.

The capacitive current i_c contains the fundamental and higher harmonics components:

$$i_c = i_{c1} + \sum_n i_{cn} \quad (2)$$

The components i_{cn} arise because of the voltage harmonics. The current i_r is also composed of fundamental and higher harmonics components:

$$i_r = i_{r1} + \sum_n i_{rn} \quad (3)$$

$$i_{rn} = i'_{rn} + i''_{rn} \quad (4)$$

Component i'_{rn} arises due to the nonlinearity of MOSA *U-I* characteristics whereas i''_{rn} arises due to presence of voltage harmonics. The magnitude of i''_{rn} depends on the peak value of voltages U_n and their phase angles Φ_n. By applying Fourier transform, the component i''_{rn} is derived from i_{rn} and the remaining component i'_{rn} is used for modelling the *U-I* characteristics of MOSA. At U_c the current through MOSA consists primarily of capacitive current and a small resistive component of non-sinusoidal current. Measured total leakage current is shown in Fig 2. and calculated resistive current in Fig 3.

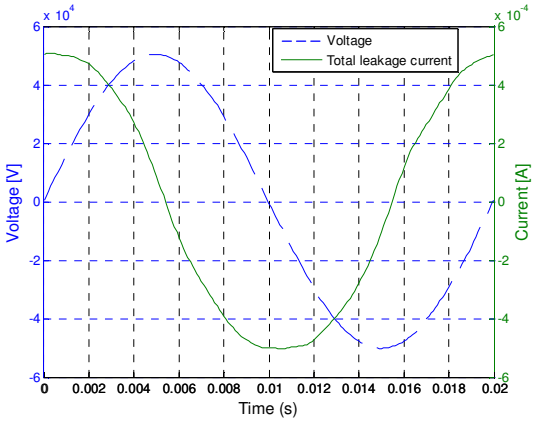

Fig. 2. Waveshapes of voltage U_c and total leakage current (peak value *I*=505.51 μA)

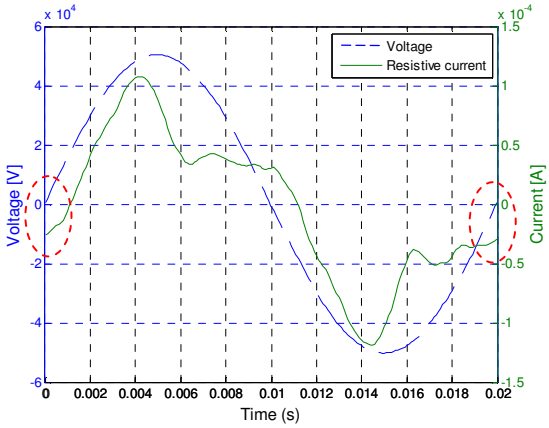

Fig. 3. Waveshapes of voltage U_c and resistive current (peak value I_R=112.51 μA)

Resistive current I_R is not symmetrical about its peak value (Fig 3.) and there is an offset at the voltage zero crossing. Therefore for this measuring point the peak of capacitive current is higher than the peak of total leakage current. The resistive component creates energy losses and increases the temperature of MOSA, compared to surrounding temperature.

Raising the voltage increases the resistive component of the current and energy losses. For AC voltage, the current waveshape changes significantly around the knee of the *U-I* characteristics, where starts the breakdown region. Measured *U-I* characteristics in per-unit of the U_r for AC voltage (50 Hz) are shown in Fig. 4.

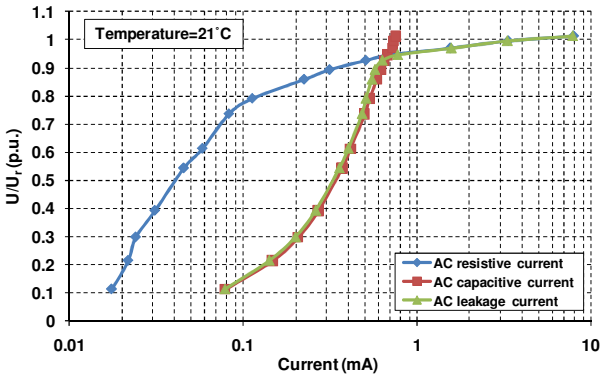

Fig. 4. Measured *U-I* characteristics

After the voltage has exceeded the knee of the *U-I* characteristic, the capacitive component becomes negligible small compared to the resistive one. For example, if rated voltage U_r is applied on MOSA, the total leakage current and its resistive and capacitive components are shown in Fig. 5, Fig. 6 and Fig. 7 respectively.

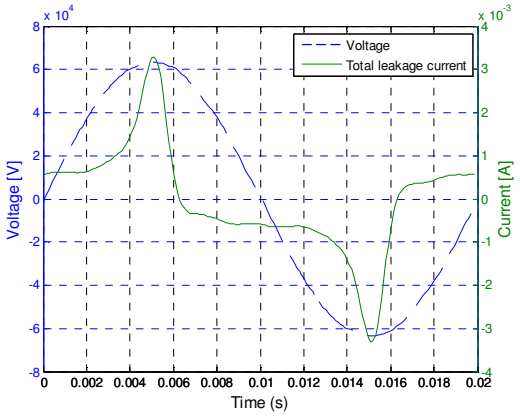

Fig. 5. Waveshapes of voltage U_r and total leakage current (peak value *I*=3.3 mA)

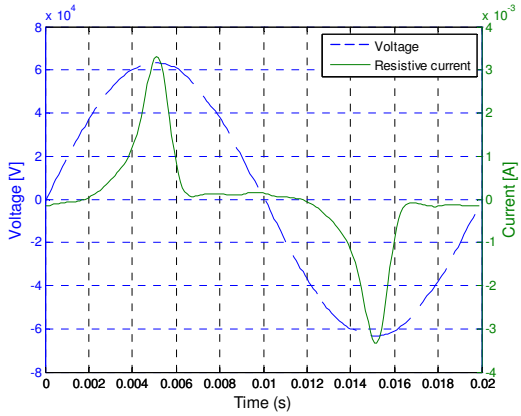

Fig. 6. Waveshapes of voltage U_r and resistive current (peak value I_R=3.3 mA)

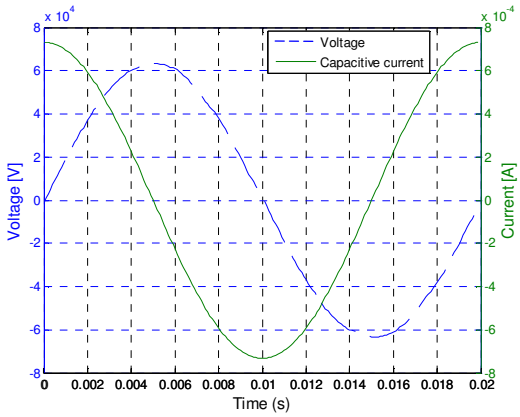

Fig. 7. Waveshapes of voltage U_r and capacitive current (peak value I_C=0.73 mA)

III. Modelling of MOSA

MOSA model used for TOV studies in EMTP-RV [4], [5] consists of nonlinear resistance defined by average U-I_R characteristic (Fig 8.) in parallel with capacitance. Average U-I_R characteristic was obtained by joining the peak values of the various U-I_R loops at different voltage levels (Fig 9.). MOSA capacitance of 35.6 pF was determined from the measurements with RLC-Meter instrument.

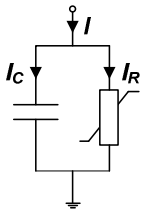

Fig. 8. MOSA model for calculation of energy stress due to TOV

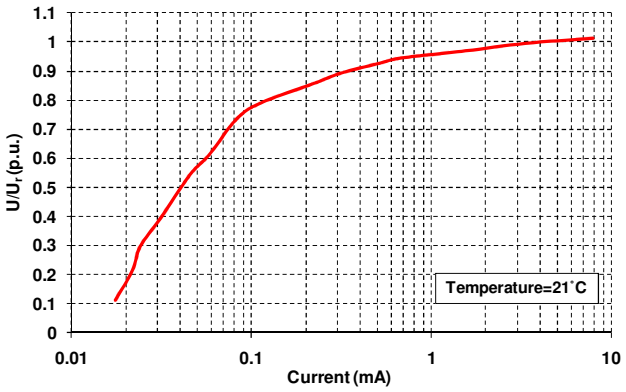

Fig. 9. Average U-I_R characteristic of MOSA

MOSA energy was calculated by using the following expression:

$$E = \int_0^t u(t) \cdot i_R(t) dt \qquad (5)$$

The energy was determined from measured voltage and resistive part of current by using trapezoidal numerical integration in MATLAB:

$$E = \sum_{k=1}^{n} \frac{u_k \cdot i_k + u_{k-1} \cdot i_{k-1}}{2} \cdot \Delta t \qquad (6)$$

MOSA energy was calculated in EMTP-RV by using expression (6) with time step Δt=100 µs. Comparison of measurement and calculation for applied voltage U_r is shown in Fig. 10. Energy waveshapes show steps because the energy increases more rapidly at the instant when resistive current and voltage reach the peak value (Fig 6.). Energy slowly increases in the area where the resistive part of current is low.

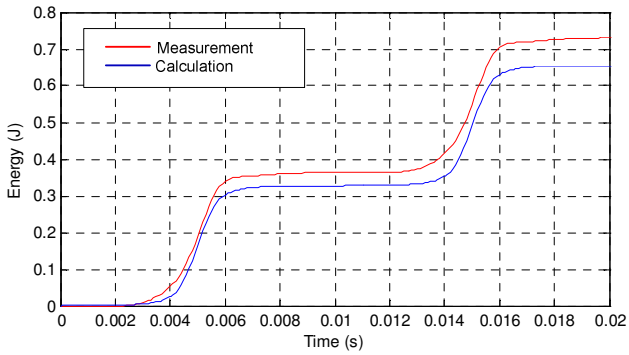

Fig. 10. Comparison of measured and calculated energy for applied voltage U_r

Difference between the results of measurement and calculation occurs due to the hysteretic behaviour of MOSA (Fig 11.).

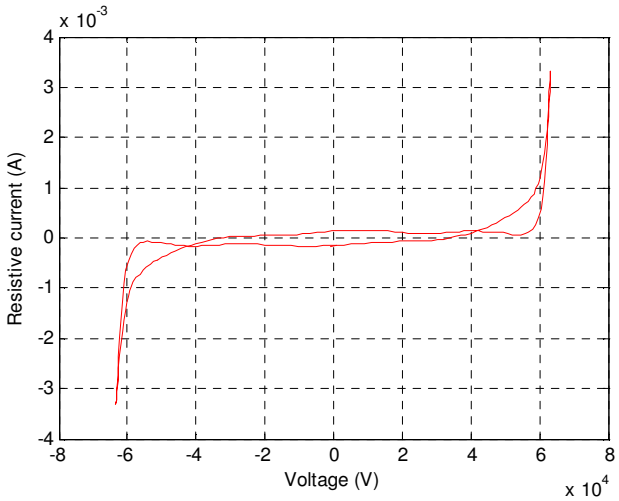

Fig. 11. Measurement of the dynamic U-I_R curve for the applied voltage U_r

The MOSA model implemented in EMTP uses the static U-I_R characteristic, which is shown in Fig 12.

The difference between the calculated and the measured resistive component of the current is shown in Fig. 13 and 14.

The hysteretic behaviour of U-I_R characteristics at different voltages is shown in Fig 15.

The influence of hysteretic behaviour on calculation of energy stress is higher in a low current region of the dynamic U-I_R characteristic and it decreases as the applied voltage across the

MOSA increases.

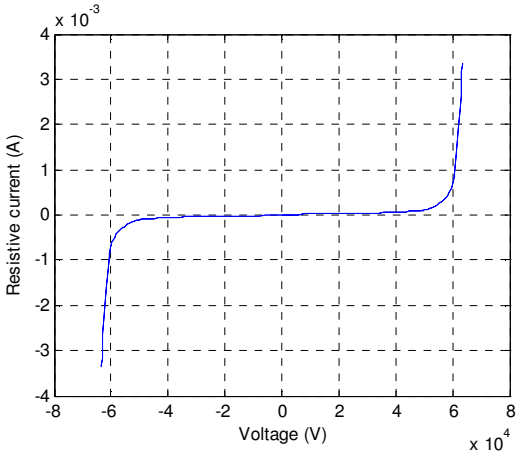

Fig. 12. Static U-I_R characteristic in EMTP for applied voltage U_r

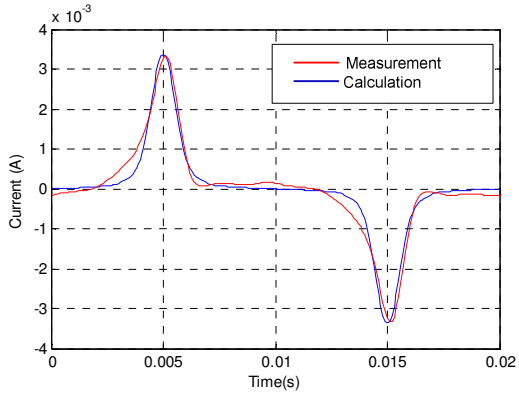

Fig. 13. Comparison of measured and calculated I_R for applied voltage U_r

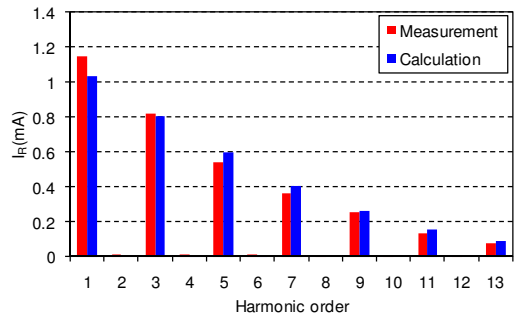

Fig. 14. Comparison of measured and calculated harmonic spectrum of I_R

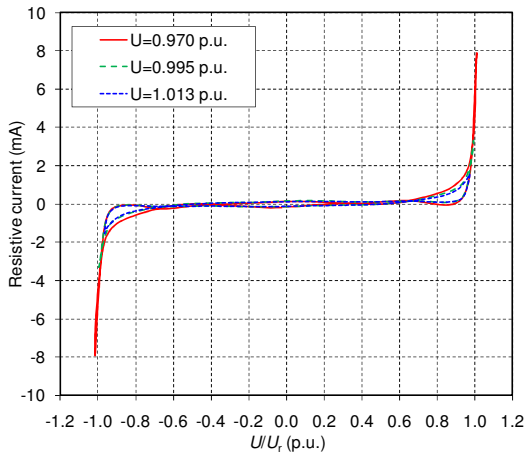

Fig. 15. Measured U-I_R characteristics at different voltages

Comparison of measurement and calculation results after t=20 ms for U/U_r >0.79 p.u. is shown in Fig 16. Results show good agreement.

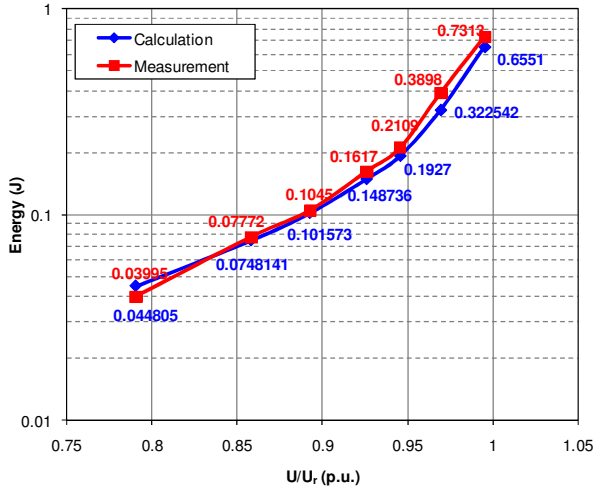

Fig. 16. Comparison of measurement and calculation for U/U_r >0.79 p.u.

The calculation of the resistive current from the total leakage current should be done when modelling MOSA for the calculation of energy at low values of TOV (low current region). Large errors in calculation of the energy stress can be obtained if the total leakage current is used for the modelling of the MOSA instead of the resistive component [6].

IV. Calculation Of TOV On Compact Lines

High voltage transmission networks can operate with directly grounded neutral of power transformers or the network may have an isolated neutral. The connection of phase conductor with the ground causes a single-phase short circuit, whereby the phase voltage increases in the "healthy" phases of the network. Guidance for the determination of TOV amplitudes is given in annex A of [7].

Voltage rise along long line due to Ferranti effect was also considered in calculations, as a cause of TOV. Sequences of causes for TOV, e.g. load rejection originating from a ground fault, need consideration, when both overvoltages have comparable severity. In such cases, however, the amount of rejected load dependent on the fault location and the MOSA location has to be carefully examined.

Combination of causes such as ground faults and load rejection may result in higher TOV values than those from the single events. When such combinations are considered sufficiently probable, the overvoltages for each cause have to be compounded taking into account the actual system configuration.

TOV analyzed in this paper combine the effect of load shedding, Ferranti effect and ground fault. Substations 1 and 2 are connected with 400 kV compact line (Fig 17). MOSAs are installed at both terminals of the line. The overhead line transmits P=300 MW and Q=130 MVAR from substation 1 to substation 2. Network with single-phase short circuit current I_{sc1}=5 kA was analyzed [8].

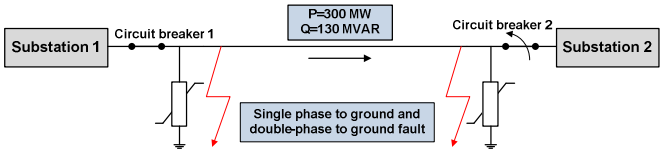

Figure 17. Model for calculation of TOVs

The following events are considered in order to evaluate the level of TOV and the effect on MOSA:

a) A single phase to ground fault in phase A occurs at the end of the line (substation 2) and then a three-phase opening of CB 2 occurs.
b) A double-phase to ground fault in phases B and C occurs at the end of the line (substation 2) and then a three-phase opening of CB 2 occurs.
c) A single phase to ground fault in phase A occurs at the entrance of the line (substation 1) and then a three-phase opening of CB 2 occurs.
d) A double-phase to ground fault in phases B and C occurs at the entrance of the line (substation 1) and then a three-phase opening of CB 2 occurs.

Analysis of MOSA energy stress due to time difference between opening of CB1 and CB2 and failure of relay protection in substation 1 is conducted. The 100 km long line considered in this paper is a single circuit 225 kV line equipped with 2 ground wires, upgraded to 400 kV without major modifications of the design of the towers. In this case the level of SFO can exceed the switching withstand voltage of the insulator strings. Sequence data of equivalent network is shown in Table I.

TABLE I
SEQUENCE DATA OF EQUIVALENT NETWORK

I_{sc1rms} (kA)	R_0/X_1	X_0/X_1	Positive sequence data (Ω)		Zero sequence data (Ω)		I_{sc3rms} (kA)
			R_1	X_1	R_0	X_0	
5	5.5	3	0	19.6	107.7	58.7	12.4

V. SELECTION OF MOSA RATED VOLTAGE

MOSA is a vital piece of equipment and an insurance against damage to the other equipment in the substation. Hence, it is essential that the MOSA itself be stable under all system operating conditions. This, in turn, requires that the system behaviour, especially under TOV conditions, be known. Selecting MOSA for a specific application is a compromise between protective level, TOV capability and energy capability. Increasing the TOV capability (by addition of blocks in series) increases the possibility of survival of the MOSA under system voltage stresses but reduces the margin of protection provided by the MOSA for a given insulation level. MOSA with a higher energy capability reduces the risk of failure. Optimization depends on how well the actual MOSA stresses are known or can be estimated. The further steps will explain how to select the parameters of MOSA. The rated voltage U_r of the MOSA should be equal to or higher than the highest equivalent TOV obtained. When protective levels lower than that of the adopted MOSA design are desired, rated voltages below the equivalent 10 s TOV may be selected, provided the MOSA is able to absorb the energy caused by system events. In this case energy absorption calculations should be carried out simulating the system events. Procedure for selection of protective levels lower than that of the adopted MOSA design is shown in Figure 18. Calculations of SFO are not presented in this paper, only TOV are considered.

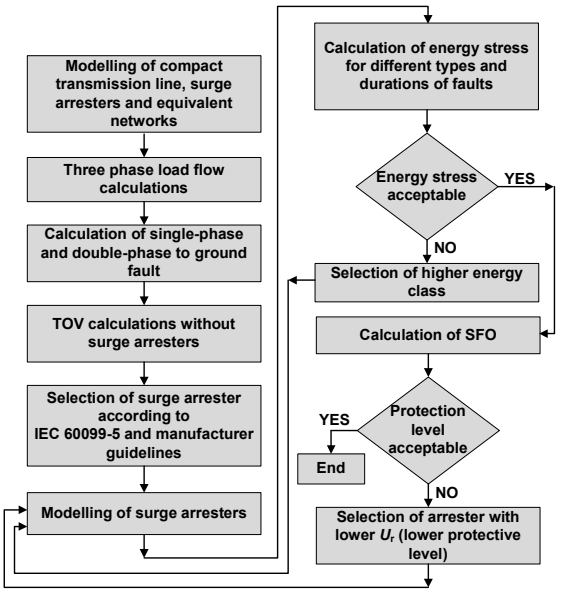

Fig. 18. Procedure for selection of protective levels lower than that of the adopted MOSA design

For the example mentioned above (Fig. 17), the MOSA with U_r=342 kV and energy class 4 (energy capability 2394 kJ) was selected according to [7]. Calculations of energy stress were carried out for the MOSA with U_r=342 kV and for the MOSA with a lower rated voltage U_r=330 kV (energy capability 2310 kJ). Static U-I_R characteristics shown in Table II were used for modelling of MOSAs in EMTP-RV.

TABLE II
STATIC U-I_R CHARACTERISTICS

Current [A]	**U_r=330 kV**	**U_r=342 kV**
	Voltage [kV]	
0.003	467	484
0.01	471	488
0.1	485	503
1	509	527
10	542	561
100	593	619
200	608	631
300	616	639
400	623	647
500	627	650
600	631	654
700	635	658
800	638	662
900	642	666
1000	644	667

VI. Simulation Results

Three-phase load flow calculation results are shown in Table III in p.u., where 1 p.u.=(420/√3)·√2=342.929 kV. Voltages at the beginning and at the end of the line before the fault occurrence are determined.

TABLE III
RESULTS OF THREE-PHASE LOAD FLOW CALCULATIONS

	U [p.u.]	φ [°]
Voltages at the beginning of the line	U_{1a}=1.0016 U_{1b}=0.9993 U_{1c}=0.9992	φ_{1a}=0.0547 φ_{1b}=-120.064 φ_{1c}=120.009
Voltages at the end of the line	U_{2a}=0.9740 U_{2b}=0.9758 U_{2c}=0.9751	φ_{2a}=-3.0686 φ_{2b}=-122.919 φ_{2c}=116.893

The results of three-phase load flow calculations are used as input parameters for the calculation of TOV caused by single-phase and double-phase to ground fault. Calculated amplitudes of TOV in the transient (U_{max}) and steady state (U_{st}) are shown in Table IV.

TABLE IV
RESULTS OF TOV CALCULATION

	a)				b)		c)				d)	
	U_{maxC}	U_{stC}	U_{maxB}	U_{stB}	U_{maxA}	U_{stA}	U_{maxC}	U_{stC}	U_{maxB}	U_{stB}	U_{maxA}	U_{stA}
	Without MOSAs											
1	1.61	1.51	1.13	1.03	1.40	1.29	1.93	1.63	1.42	1.28	1.66	1.41
2	1.54	1.45	1.15	1.02	1.36	1.29	1.91	1.73	1.52	1.38	1.57	1.47
3	1.88	1.59	1.38	1.25	1.62	1.38	1.58	1.49	1.17	1.07	1.40	1.28
4	1.68	1.52	1.40	1.18	1.49	1.37	2.06	1.74	1.66	1.39	1.83	1.48
	MOSAs with U_r=342 kV											
1	1.58	1.51	1.13	1.03	1.40	1.29	1.81	1.63	1.40	1.28	1.64	1.41
2	1.53	1.45	1.14	1.02	1.36	1.29	1.78	1.72	1.40	1.38	1.57	1.47
3	1.79	1.59	1.37	1.25	1.61	1.38	1.54	1.49	1.17	1.07	1.40	1.28
4	1.65	1.51	1.38	1.18	1.49	1.37	1.82	1.73	1.45	1.40	1.76	1.48
	MOSAs with U_r=330 kV											
1	1.56	1.51	1.13	1.03	1.42	1.29	1.76	1.63	1.39	1.28	1.62	1.41
2	1.52	1.45	1.13	1.02	1.36	1.29	1.73	1.71	1.42	1.41	1.56	1.47
3	1.74	1.59	1.36	1.25	1.59	1.38	1.52	1.49	1.17	1.07	1.39	1.28
4	1.63	1.51	1.37	1.18	1.49	1.37	1.75	1.71	1.48	1.45	1.72	1.48

Voltages are expressed as p.u. values for the following cases: 1 – beginning of the line during the fault; 2 – beginning of the line after opening of CB 2; 3 – end of the line during the fault; 4 – end of the line after opening of CB 2. Analyses of maximum TOV values in phases B and C for different times of fault occurrence in phase A were conducted. For case c) maximum voltages in phases C and B are computed in each simulation, in order to find the time of single-phase to ground fault occurrence at which the overvoltages are the highest. Event c) represents the most severe event regarding energy stressing of MOSAs. Results of TOV calculations are shown in Figs 19 - 22. Figures 23, 24 and 25 show the energy stress and the currents through the MOSAs with the rated voltage U_r=330 kV for case c) in substation 2. The energy stressing the MOSAs with the rated voltages 342 kV and 330 kV versus the duration of the fault and the time after the opening of the CB 2 is shown in Table V. Energy stress and currents through MOSA at the end of the line are higher in the period after opening of CB 2 than during the fault.

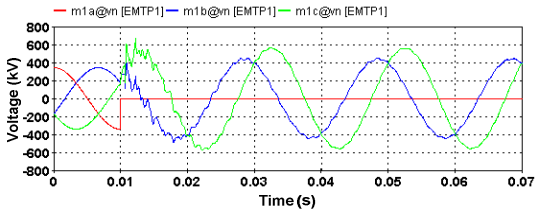

Fig. 19. Voltages at the beginning of the line during single-phase short circuit

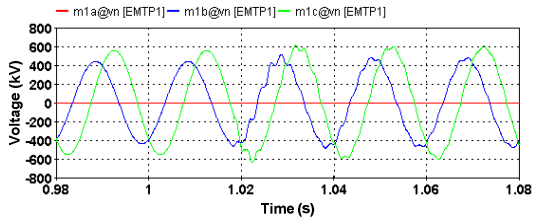

Fig. 20. Voltages at the beginning of the line after opening of CB 2

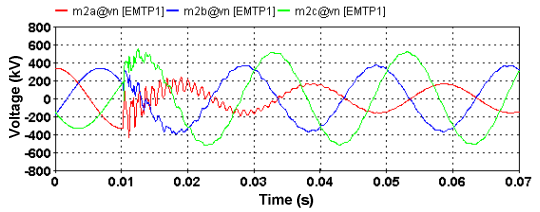

Fig. 21. Voltages at the end of the line during single-phase short circuit

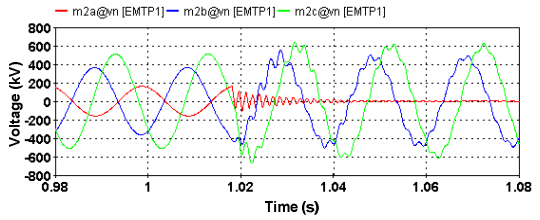

Fig. 22. Voltages at the end of the line after opening of CB 2

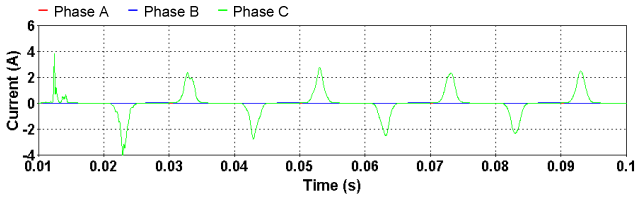

Fig. 23. Currents through MOSAs at the end of the line during the fault

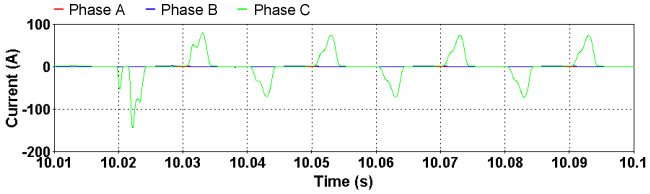

Fig. 24. Currents through MOSAs at the end of the line during fault and after opening of CB 2 (t_{open}=10.02 ms)

Energy stress of MOSA in phase C at the end of the line increases rapidly after opening of CB 2 at t_{open}=10.02 ms (Fig. 25) due to combined TOV - earth fault and Ferranti effect.

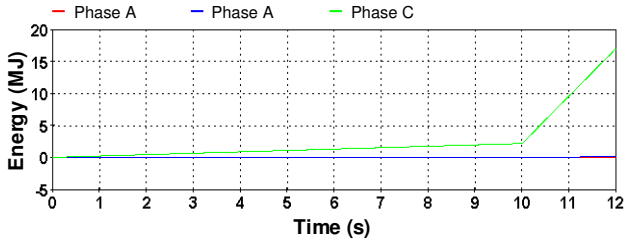

Fig. 25. Energy stressing the MOSA in phase C at the end of the line during the fault and after opening of CB 2 (t_{open}=10.02 ms)

TABLE V
RESULTS OF MOSA ENERGY STRESS [KJ/S] VERSUS TIME

U_r (kV)	Energy capability (kJ)	a)	b)	c)	d)
330	2310	Beginning of the line during the fault			
		285.03	8.636	1823.1	63.601
		Beginning of the line after opening CB2			
		112.75	9.316	**7561.8**	150.01
		End of the line during the fault			
		942.79	34.612	197.44	7.8565
		End of the line after opening of CB 2			
		309.75	33.73	**8298.8**	175.846
342	2394	Beginning of the line during the fault			
		126.185	2.3992	793.81	24.833
		Beginning of the line after opening CB2			
		47.48	2.6309	3277.5	64.714
		End of the line during the fault			
		424.51	12.2792	85.967	2.1352
		End of the line after opening of CB 2			
		138.39	11.924	3759.2	76.855

The combination of maximum allowed duration of fault versus maximum allowed time after opening of CB in substation 2, for which the MOSA would stand the energy stress is shown in Fig 26.

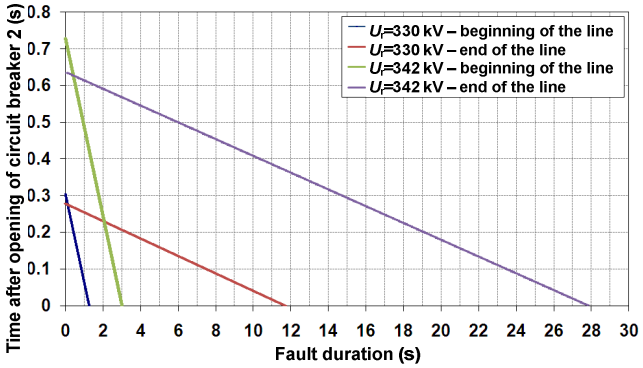

Fig. 26. Fault duration versus time after opening of CB 2

If the duration of fault (relay protection settings) is known, from Fig 26. it is easy to determine whether the energy capability of the MOSA is exceeded. In the case c) the energy capability of MOSA with U_r=330 kV at the beginning of the line will be exceeded if the fault is not eliminated in both substations in less than 1.27 s (Fig 26). If the fault is eliminated in substation 1 (relaying problem) for example in 300 ms, the energy capability of MOSA will be exceeded if time after opening of CB 2 is greater than 233 ms. The energy capability of MOSA will be exceeded for the combination of times that lie above the curves.

VII. CONCLUSIONS

This paper describes a procedure for the calculation of the MOSA energy stress during TOV. Laboratory measurements were conducted and a MOSA model was developed in EMTP-RV software. Comparisons between measured and calculated MOSA energy showed a good agreement.

A method for the selection of protective levels lower than that of the adopted MOSA design was described. By using this method MOSA with low protection level can be selected without being overstressed by TOV, and, therefore, overvoltage protection of compact line can be improved. According to [7] a MOSA with a rated voltage U_r=342 kV was selected. Calculation results show that the MOSA with U_r=330 kV could also be selected without being overstressed by TOV, for certain durations of TOV. This MOSA has a lower protection level and it reduces SFO and fast-front overvoltages more efficiently.

After the selection of the MOSA according to the shown procedure, the study could be performed in order to check if the SFO are reduced to a level acceptable for the compact line. Another alternative for the limitation of SFO is the application of transmission line arresters that can be located along the line at selected points to obtain an adequate overvoltage profile along the line [9] [10].

VIII. REFERENCES

[1] A. Legate, J. Brunke, J. Ray, E. Yasuda, "Elimination of closing resistors on EHV Circuit Breakers", *IEEE Trans. Power Delivery*, Vol. 3, No. 1, January 1988, p. 223.

[2] J. Ribeiro, M. McCallum, "An application of metal-oxide surge arresters in the elimination of need for closing resistors in EHV breakers", *IEEE Trans. Power Delivery*, Vol. 4, No. 1, January 1989, p. 282.

[3] H. Zhu, M. R. Raghuveer, "Influence of representation model and Voltage Harmonics on Metal Oxide Surge Arrester Diagnostics", *IEEE Trans. Power Delivery*, Vol. 16, No. 4, October 2001.

[4] J. Mahseredjian, S. Dennetière, L. Dubé, B. Khodabakhchian and L. Gérin-Lajoie: "On a new approach for the simulation of transients in power systems". Electric Power Systems Research, Vol. 77, Issue 11, September 2007, pp. 1514-1520.

[5] J. Mahseredjian, C. Dewhurst, "Using EMTP Tutorials and Reference", Hydro-Québec/IREQ, 2007.

[6] G. R. S. Lira, D. Fernandes Jr. and E. G. Costa "Computation of Energy Absorption and Residual Voltage in Metal Oxide Surge Arrester from Digital Models and Lab Tests: A Comparative Study", *IPST*, Lyon, France, June 4-7, 2007.

[7] IEC 60099-5: "Surge arresters – Part 5: Selection and application recommendations", Edition 1.1, 2000.

[8] B. Filipović-Grčić, I. Uglešić, A. Xemard, "Selection of station surge arresters for control of slow-front overvoltages on compact lines", *CIGRE C4 Colloquium on: Lightning and Power Systems,* Kuala Lumpur, Malaysia, 2010. pp. 1-14.

[9] H. Seyedi, M. Sanaye-Pasand, M. R. Dadashzadeh, "Application of Transmission Line Surge Arresters to Reduce Switching Overvoltages", *IPST*, Montreal, Canada on June 19-23, 2005, Paper No. IPST05 – 082.

[10] L. Stenström, M. Mobedjina, "Limitation of switching overvoltages by use of transmission line surge arresters", ABB Switchgear Sweden, *SC 33 International conference* CIGRE, Zagreb, Croatia 1998.